Title: **Structural basis of connexin-36 gap junction channel inhibition**

Xinyue Ding[1], Simone Aureli[2,3], Anand Vaithia[1], Pia Lavriha[1], Dina Schuster[4,5], Basavraj Khanppnavar[1], Xiaodan Li[1], Thorsten B. Blum[1], Paola Picotti[4], Francesco L. Gervasio[2,3,6,7*], Volodymyr M. Korkhov[1,5,*]

[1] Laboratory of Biomolecular Research, Paul Scherrer Institute, Villigen, Switzerland

[2] School of Pharmaceutical Sciences, University of Geneva, CH-1211 Geneva, Switzerland

[3] ISPSO, University of Geneva, CH-1211 Geneva, Switzerland

[4] Institute of Molecular Systems Biology, ETH Zurich, Switzerland

[5] Institute of Molecular Biology and Biophysics, ETH Zurich, Switzerland

[6] Department of Chemistry, University College London, WC1E 6BT London, UK

[7] Swiss Institute of Bioinformatics, University of Geneva, Geneva, CH-1206, Switzerland

* Corresponding authors:
Francesco.Gervasio@unige.ch and volodymyr.korkhov@psi.ch

Abstract: Connexin gap junction channels and hemichannels play important roles in intercellular communication and signaling. Some of connexin isoforms are associated with diseases, including hereditary neuropathies, heart disease and cancer. Although small molecule inhibitors of connexins show promise as therapeutic agents, the molecular mechanisms of connexin channel inhibition are unknown. Here, we report the cryo-EM structure of connexin-36 (Cx36) bound to an anti-malarial drug mefloquine at 2.1 Å resolution. Six drug binding sites partially occlude the pore of each connexon forming the channel. Each drug molecule in the ring makes contacts with residues in the pore-lining pocket and with the neighbouring mefloquine molecules, partially occluding the pore and modifying the pore electrostatics, ultimately reducing solute translocation through the channel. Structures of Cx36 in the presence of quinine and quinidine show a similar mode of drug binding. Molecular dynamics simulations of Cx36 bound to mefloquine show that drug binding affects the kinetics of ion passage through the pore. This previously undescribed mode of connexin channel inhibition presents an opportunity for designing subtype-specific connexin inhibitors.

One-sentence summary: Mechanism of connexin channel inhibition by small molecules

Introduction

Connexins enable direct communication between cells in a tissue by forming hexameric connexons or hemichannels (HCs), which reach the cellular surface and dock with their counterparts on the neighbouring cells [1]. The resulting assemblies, known as gap junction channels (GJCs), span two plasma membranes and couple the neighbouring cells metabolically and electrically [2,3]. The GJCs play a crucial role in many physiological processes, such as cardiac and smooth muscle contractility (Cx43) [4,5], action potential propagation (Cx43) [6,7], neuronal synchronization (Cx36) [8,9], or insulin secretion (Cx36) [10]. Different GJCs also take an active role in cell growth and differentiation, tissue development and homeostasis [11], and disruptions of connexin function can lead to severe pathological conditions. For example, dysfunctions in different connexin channels have been linked to deafness (Cx26) [12], cataracts (Cx46 and Cx50) [13], peripheral neuropathy (X-linked Charcot-Marie-Tooth disease, Cx32) [14], cardiac arrhythmias (Cx40 and Cx43) [15,16] and various forms of cancer [17].

Due to their importance in health and disease, connexins are recognized as prospective targets for therapeutic interventions. While etiology of connexin-associated diseases in many cases likely involves disrupted intercellular communication [18-20], blockage of connexin GJC-mediated intercellular communication or HC-mediated substrate secretion is highly desirable as a therapeutic strategy in wound healing or in cancer treatment [21,22]. Several compounds inhibit GJCs and HCs non-specifically. For example, carbenoxolone, oleamide, anandamide, 2-APB have been shown to inhibit multiple connexin isoforms[23-26]. It is worth noting that the binding affinity of any of these drugs for the channels has not been well established for lack of suitable tools / reagents, and much of what we know about the drug potency today is based on channel activity inhibition. Understanding the molecular mechanisms of connexin channel activity and small molecule-mediated inhibition will be essential for designing novel drugs with high specificity for different connexin isoforms, potentially offering more effective treatments to those currently available.

Cx36 is a major connexin isoform in the pancreas and in the brain [10,27]. The physiological function of Cx36 in these tissues is to regulate neuronal activity and to mediate insulin secretion. Dysregulation of Cx36 has been associated with several human disorders. Notably, overexpression and heightened connectivity of neuronal Cx36 gap junctions has been observed in patients suffering from epilepsy, following traumatic brain injury and ischemia [28]. The elevated gap junction coupling in these conditions contributes to subsequent neuronal death. Furthermore, in conditions such as amyotrophic lateral sclerosis (ALS), inhibiting Cx36 by pharmacological or genetic means has shown to confer neuroprotection [29]. Therefore, development of selective inhibitors of Cx36 could be of therapeutic value. Although a cryo-EM structure of Cx36 has been solved recently, providing important insights into its molecular gating [30], it remains unclear how exactly drugs (or any other agents) inhibit the channel. It is also worth noting that the structural basis of drug-mediate inhibition not only in Cx36 but also in other connexins has remained unresolved to date.

69 Three anti-malarial drugs, mefloquine, quinine and quinidine (an enantiomer of quinine; **Figure 1a-b**),
70 inhibit Cx36 channel with high specificity and with high apparent affinity [31-33]. The mechanism of action
71 of these drugs has been suggested to involve the *Plasmodium falciparum* 80S ribosome as the primary
72 target (as in the case of mefloquine) [34]. However, alternative research has pinpointed another intriguing
73 target for mefloquine and quinine: *P. falciparum* purine nucleoside phosphorylase (PfPNP) [35].
74 Mefloquine has been shown to cause severe cardiac, neurological and psychiatric side-effects [36-38].
75 Quinine is known to cause cardiovascular side effects, blood disorders and cinchonism, a neurological
76 disorder linked to cinchona bark intoxication (cinchona is a natural source of quinine) [39]. Interestingly,
77 quinidine is used clinically not only as an anti-malarial but also as an anti-arrhythmic drug, e.g. in
78 treatment of the Brugada syndrome [40]. The molecular mechanisms underlying the side effects of these
79 drugs are not known and may involve multiple cellular targets, but it is likely that Cx36 inhibition and
80 disruption of gap junction-mediated cell coupling play a role.

81 We set out to characterize the structure of Cx36 in the absence and in the presence of mefloquine,
82 quinine and quinidine, and to determine the general principles of connexin channel inhibition by small
83 molecules.

84

Results

Purified Cx36 binds to anti-malarial drugs *in vitro*. We expressed and purified the human Cx36 in detergent micelles (Extended Data Fig. 1a-b) and performed tryptophan fluorescence quenching-based ligand binding assays (Extended Data Fig. 1e-g, Extended Data Fig. 2). The experiments showed that all three drugs have micromolar affinity for the protein, with mefloquine binding to Cx36 with the highest apparent K_d value (**Figure 1c**). Experiments utilizing the nano-differential scanning fluorimetry (nano-DSF) technology showed a similar result, with an estimated K_d for mefloquine in the micromolar range (Extended Data Fig. 1h). These experiments confirmed that the drugs of interest interact with the purified Cx36 *in vitro* with micromolar affinity, suggesting a useful range of the drugs for our structural study.

Structure of Cx36 in the absence and in the presence of drugs. The expressed and purified Cx36 was applied to the cryo-EM grids (in the absence or in the presence of the drugs of interest at a final concentration of 1 mM), plunge-frozen in liquid ethane and subjected to cryo-EM analysis. The acquired movies were processed as described in Materials and Methods, resulting in three reconstructions: Cx36-mefloquine at 2.14 Å resolution (Cx36-mfq; **Figure 1d-e**, Extended Data Fig. 3), Cx36-quinine at 2.73 Å resolution (Cx36-quin; **Figure 1e**, Extended Data Fig. 4), and Cx36-quinidine at 2.9 Å resolution (Cx36-quid; **Figure 1e**, Extended Data Fig. 5). The apo-Cx36 sample was prepared and analysed in a similar way, in the absence of any added compounds, resulting in a refined cryo-EM map of Cx36 at 2.49 Å resolution (apo-Cx36; **Figure 1e**, Extended Data Fig. 6, Extended Data Table 1).

The four structures show the architecture of the Cx36 GJC (**Figure 1d-e**), consistent with the recently published Cx36 in detergent and in nanodisc environment [30]. In our case, the N-terminal gating helix is unresolved in each of the four structures (Extended Data Fig. 7b). It is possible that in the detergent environment the N-terminal helix is too dynamic to be captured by cryo-EM. Overall, the protein conformations in the three structures are nearly identical (Extended Data Fig. 7-8). The major differences were found in the pore region: the Cx36-mfq, Cx36-quin, and Cx36-quid feature an additional density, corresponding to a bound drug (**Figure 1e**, **Figure 2**, Extended Data Fig. 7c). Six copies of the drug are bound within the six sites in each connexon of the Cx36 GJC (**Figure 2a, c, e**).

Details of the binding site. The structures of Cx36-mfq, Cx36-quin and Cx36-quid reveal three key elements of the drugs, relevant to connexin channel interactions: (i) a planar group that inserts into the pocket formed by residues in the transmembrane helices TM1 and TM2 (we refer to this moiety as the "body"); (ii) a hydrophobic "head-group", which extends into the pore and makes lateral contacts with the neighbouring drug molecules; (iii) a nitrogen atom within the headgroup that contacts the conserved negatively charged residue at the periphery of the pocket (E43 in Cx36) (**Figure 2a, c, e**).

119 The resolution of our Cx36-mfq 3D reconstruction gives the greatest insight into the atomic details of
120 inhibitor binding. The body of the drug wedges itself into the pocket at the interface of two Cx36
121 monomers, interacting with the residues I35, V38, A39 and I40 in TM1, and I76, V80, I83 and I84 in
122 TM2 (**Figure 2b**). I40 from the neighbouring Cx36 monomer contributes to the hydrophobic pocket.
123 The pocket is hydrophobic, and it is likely that multiple weak non-polar interactions and geometric
124 complementarity between mefloquine and the pocket drive this interaction. The piperidinium head-
125 group of mefloquine is asymmetrically extending toward the pore. The binding pose of mefloquine is
126 stereoselective: although we used a racemic mixture of the drug for sample preparation, the high
127 resolution structure captured the S,R-enantiomer of mefloquine (**Figure 2a-b**). The hydrophobic
128 headgroup is stabilized by an interaction with the carboxyl of the residue E43 in the pore (**Figure 2b**).
129 Moreover, the N atom of the piperidinyl group in mefloquine is within a close distance from E43
130 carboxyl, and the O atom of the neighbouring hydroxyl in the drug molecule is linked to E43 via an
131 ordered water molecule (**Figure 2b**).

132 In the case of the quinine- and quinidine-bound Cx36, the bound drugs are somewhat less well resolved
133 at the nominal resolution of 2.73 Å and 2.9 Å (compared to mefloquine, where the head-group ring is
134 clearly visible in the 2.14 Å cryo-EM map). This disparity in the drug density may be attributed to the
135 lower K_d of quinine/quinidine binding to Cx36 compared to mefloquine. Nevertheless, the density map
136 quality allows us to confidently model the drugs based on the observed features (**Figure 2c, e**). In both
137 cases the body of the drug engages in fewer hydrophobic contacts, and very distinct head-group is
138 pointing towards the pore and making contacts with the neighbouring ligand head-group and with the
139 E43 residue (**Figure 2d, f**). Although quinine and quinidine are stereoisomers, each appears to be
140 readily accommodated within its binding site inside the Cx36 pore.

141 A combination of the hydrophobic pocket-bound ligand body, polar interactions of E43 carboxyl with
142 the ligand head, and lateral packing of six neighbouring mefloquine molecules against each other within
143 the Cx36 pore generates a hydrophobic ring in the translocation pathway (**Figure 3a**). Despite leaving
144 an apparent wide aperture within the pore, the six bound mfq or quinine molecules suffice to perturb
145 the channel function of Cx36. In the case of quinidine, the drug in the observed conformation
146 completely closes the pore. It is worth noting that although we modelled the ligands according to the
147 features of the experimentally determined density maps (**Figure 2c, e**), we can not exclude that
148 alternative conformations of the ligand head-groups may exist.

149 **Small molecule binding site in other connexin isoforms.** The important feature of the observed
150 binding site is the relatively poor conservation of the residues lining the pocket, despite the structural
151 conservation of the connexin (Extended Data Fig. 9a-b). The residues lining the drug binding site in
152 Cx36 vary substantially in other connexins. Interestingly, in the X-ray- and cryo-EM-based 3D
153 reconstructions of other connexin channels, this pocket is almost always filled by densities consistent
154 with bound lipids or detergents (Extended Data Fig. 9c). While this site in distinct connexin channels

155 interacts non-specifically with hydrophobic small molecules, our structures show that this site is used
156 by connexin-specific drugs.

157 **Molecular dynamics simulations of Cx36 inhibition by mefloquine.** To shed light on the dynamic
158 behavior of the mefloquine-bound Cx36 complex and its impact on ion permeation, we performed
159 molecular dynamics (MD) simulations. We ran 300 ns-long MD simulations of the *apo* and *holo*
160 structures of Cx36 HC (*apo-Cx36* and *6mfq-Cx36* hereafter, **Figure 3b**). The low average Root Mean
161 Square Deviation (RMSD) values (~1.0 Å; Extended Data Fig. 10a) of the secondary structure Cα atoms
162 during the simulation indicate a good conformational stability for both systems, suggesting that the
163 presence of six ligands has a negligible impact on the overall Cx36 conformational plasticity. This was
164 also confirmed by the per-residue Root Mean Square Fluctuations (RMSF; Extended Data Fig. 10b-c),
165 and by a RMSD-based cluster analysis carried out on the Cx36 hexamer in the two systems (cut-off 1.5
166 Å). Notably, a single largely populated cluster family (containing >75% of the trajectory's frames) was
167 identified for both *apo-Cx36* and *6mfq-Cx36.* A superimposition of the centroids on the secondary
168 structure's Cαs showed a RMSD of ~2.0 Å (see Extended Data Fig. 10d), in line with our hypothesis
169 of negligible impact of the six ligands on the protein's conformational plasticity.

170 **Dynamics of the Cx36-bound mefloquine.** Having established that the structure and dynamics of
171 Cx36 in the absence and in the presence of drug did not change dramatically, we focused on the six
172 bound mefloquine molecules. As displayed in **Figure 3c**, mefloquine establishes predominantly
173 hydrophobic interactions with the amino acids of two adjacent Cx36 monomers, eased by the presence
174 of mefloquine trifluoromethyl groups ("body"). While these interactions stabilize the ligands in their
175 own binding pockets, they still allow mefloquine to exhibit a substantial conformational freedom during
176 the MD simulations. To quantify this behavior, we carried out a cluster analysis on each of the
177 mefloquine molecules (cutoff 1.5 Å; see Extended Data Fig. 10e). This analysis revealed the presence
178 of two main conformations, i.e. *C1* (**Figure 3d**) and *C2* (**Figure 3e**). While *C1* presents the mefloquine
179 binding mode superimposable to our cryo-EM-derived structure (featuring the mefloquine "head-
180 group" piperidinyl within a close distance from E43 carboxyl), *C2* loses the E43-mediated interaction,
181 pointing its headgroup towards the Cx36 hexamer's internal cavity.

182 **Effects of mefloquine on ion movement through the pore.** To evaluate the impact of the mefloquine
183 molecules occupying their six binding sites in Cx36 on ion translocation, we conducted a comparative
184 analysis of the number of K^+ and Cl^- ions traversing the hemichannel in both *apo-Cx36* and *6mfq-Cx36*
185 MD simulations. As shown in Extended Data Table 2, the passage of K^+ and Cl^- ions was inhibited by
186 the drug. Over the course of our simulations, we measured 30 full K^+ and 6 Cl^- transitions in the *apo-*
187 *Cx36* simulation whereas only 7 K^+ and 2 Cl^- were observed in the *6mfq-Cx36*. These results provide
188 qualitative hints about the effect of the mefloquine molecules bound to their pockets in the Cx36 on ion
189 permeation, where the ligands seem to influence the ion translocation pathway. Interestingly, the

translocation pathway is not completely sterically blocked, indicating that the pore properties must be affected to cause the reduction in ion permeability.

Free energy associated with ions permeation. To quantify the impact of mefloquine on ion permeation through Cx36, we employed a collective-variable (CV)-based free energy algorithm known as On-the-fly Probability Enhanced Sampling (OPES). This method enables the sampling of ion crossings and associated free energy profiles. Notably, OPES stands out among other CV-based enhanced sampling approaches by swiftly constructing a bias potential through on-the-fly probability estimation along selected CVs, ensuring an optimal equilibrium between exploration and convergence [41].

We performed two OPES simulations for 300 ns on the *apo-Cx36* system sampling the permeation of both K^+ and Cl^- (*apo-Cx36_*K^+ and *apo-Cx36_*Cl^-, respectively). Other two 300ns-long OPES simulations were carried out on the *6mfq-Cx36* system to investigate ion translation (*6mfq-Cx36_*K^+ and *6mfq-Cx36_*Cl^-; detailed in the Materials and Methods and in Extended Data Fig. 11a). As shown in Extended Data Fig. 11b, the free-energy profile of K^+ in the *apo-Cx36* and in the *6mfq-Cx36* simulations strongly differs at the level of the transition state (D_{up}~3.0 nm), where the mefloquine ligands are located. On the contrary, the free-energy of the two main basins (D_{up}~1.5 nm and D_{up}~4.0 nm) appears unaffected by mefloquine ligands, as indicated by a consistent difference of approximately 2.0 kcal/mol measured over the OPES simulation time (see Extended Data Fig. 11d). Similar scenario can also be observed for the permeation free-energy of Cl^-, whose profile differs around the value of D_{up}~1.5-3.0 nm between the *apo-Cx36_*Cl^- and *6mfq-Cx36_*Cl^- OPES simulations (Extended Data Fig. 11c). Instead, the two basins at D_{up}~1.0 nm and D_{up}~4.0 nm are almost identical in value, and their difference along the computational time is measured to be ~-1.7 kcal/mol (Extended Data Fig. 11e).

These results indicate that the six mefloquine molecules inhibit Cx36 by acting on the kinetics of the ion permeation instead of affecting the thermodynamics of the process. This may be due to a combined effect of (i) a modest decrease of the Cx36 pore size upon mefloquine binding, and (ii) dramatic changes in the electrostatic potential of the pore. These effects likely force the passing ions to lose their hydration shells in order to pass through the pore. To verify this suggestion, we reweighted the collected bias potential on the "Hydration shell" CV, to monitor the amount of water surrounding the ions during the crossing the Cx36 hexamer (detailed in Materials and Methods). As shown in **Figure 3f-g**, the K^+ and Cl^- ion lose more than the 50% of their hydration shells while moving across the pore in the *6mfq-Cx36_*K^+ *and 6mfq-Cx36_*Cl^- OPES simulations. It is worth mentioning that the Cl^- ions can exhibit a variety of hydration values in the intracellular side of the hexamer cavity, ranging from "fully hydrated" (~0.9) to "poorly hydrated" (~0.4) on a scale from 0 to 1. Such behavior, distinct from that of the K^+ ion, seems to be due to the presence of a pronounced positive electrostatic potential on the intracellular side of Cx36 hexamer, inducing Cl^- ion-protein surface interactions (Extended Data Fig. 11f). Thus,

225 while our simulations show that a complete channel blockage does not occur, consistent with the cryo-
226 EM structure, the flux of ions is substantially reduced upon mefloquine binding.

227

228 **Discussion**

229 Ion channel-targeted drug development is a major area of medicinal chemistry and pharmacology.
230 Many of the drugs on the market or in phase II/III trials today target ligand- and voltage-gated ion
231 channels, such as benzodiazepine diazepam [42], verapamil [43] and AXS-05 [44]. The importance of ion
232 channels for drug discovery is also exemplified by the absolute requirement to test all newly developed
233 drugs for cross-reactivity with HERG channel to prevent cardiotoxicity [45]. Connexin channels,
234 including GJCs and HCs, also represent attractive drug targets and new therapies acting on Cx26 and
235 Cx43 are currently under development [46]. Some of the known drugs with primary action unrelated to
236 connexins (such as mefloquine, quinine and quinidine, the topic of this study) cross-react with Cx36.
237 This reactivity may underlie the adverse effects of these drugs. The neurological and cardiac effects of
238 all three drugs may well correlate with the ability of these drugs to disrupt gap junction coupling in the
239 brain or heart, respectively. Moreover, this may be an effect mediated by Cx36 or by other connexin
240 channels that may be able to accommodate these drugs similarly in the pore binding sites.

241 The Cx36-bound drugs are sufficiently well resolved in our cryo-EM reconstructions, allowing us to
242 get a glimpse into the atomic details of the drug-protein interaction. The mode of drug-connexin
243 interaction relies not only on the complementarity between the drug and the protein pocket, but also on
244 the geometry and physical properties of the drug itself. The neighbouring drug molecules within the
245 pore interact with each other, forming a hydrophobic ring within the pore that either obstructs the pore
246 completely or introduces the electrostatic barrier that limits solute translocation through the channel
247 (**Figure 4**).

248 The mode of connexin inhibition by the small molecules described here is unique among the ion
249 channels, and it presents an attractive new approach to tackle the challenge of drug discovery aimed at
250 specific connexin isoforms. The following criteria would have to be satisfied to develop a connexin
251 subtype-selective inhibitor: (i) extensive contacts and high complementary to the drug pocket ("body");
252 (ii) the presence of an asymmetric drug "head-group" mediating the contacts with the neighbouring
253 drugs and with the conserve carboxyl (equivalent to E43 in Cx36). These features could build on the
254 existing geometry and the principles of anti-malarial drug-mediated inhibition as described here,
255 although it can be foreseen that other solutions can be found utilizing the same binding site but very
256 different chemistry. Headgroup modification could potentially be used to fine-tune the permeability of
257 the channels. This may be possible to accomplish due to the incomplete blockage of the channel by the
258 drugs, evident from our structures and MD simulations. Both the strength of drug-drug interactions in

259 the connexin pore and the permeability of the drug-bound state of the channel to small solutes or ions
260 may be possible to tailor to the specific connexin isoforms.
261

Acknowledgements

We thank Miroslav Peterek and Bilal Qureshi (ScopeM, ETH Zurich) for expert support in cryo-EM data collection. We also thank Spencer Bliven and Marc Caubet-Serrabou (PSI) for the support in high performance computing. We thank Richard Kammerer (PSI) for critical feedback on the manuscript. The work was supported by the Swiss National Science Foundation grant 184951 (VMK).

Competing interests

Authors declare that they have no competing interests.

Data and materials availability

The atomic coordinates will be deposited in the Protein Data Bank; the density maps will be deposited in the Electron Microscopy Data Bank with the following accession numbers: PDB ID 8QOJ, EMD-18540; PDB ID 8R7P, EMD-18987; PDB ID 8R7Q, EMD-18988; PDB ID 8R7R, EMD-18989. All other data are available in the main text or the supplementary materials.

Author contributions

X.D. planned and performed the experiments, analyzed the data, wrote the manuscript, S.A. performed the simulations, analyzed the data, wrote the manuscript, A.V. performed the experiments, analysed the data, wrote the manuscript, P.L. performed the experiments, analyzed the data, D.S. performed the experiments, analyzed the data, B.K. performed the experiments, analysed the data, X.L. analysed the data, T.B.B. analysed the data, P.P. provided resources, instrumentation and methodology, F.L.G. conceptualized the study, planned and analyzed the simulations, wrote the manuscript, V.M.K. conceptualized the study, planned and performed the experiments, analyzed the data, wrote the manuscript.

287 **Figures**

288

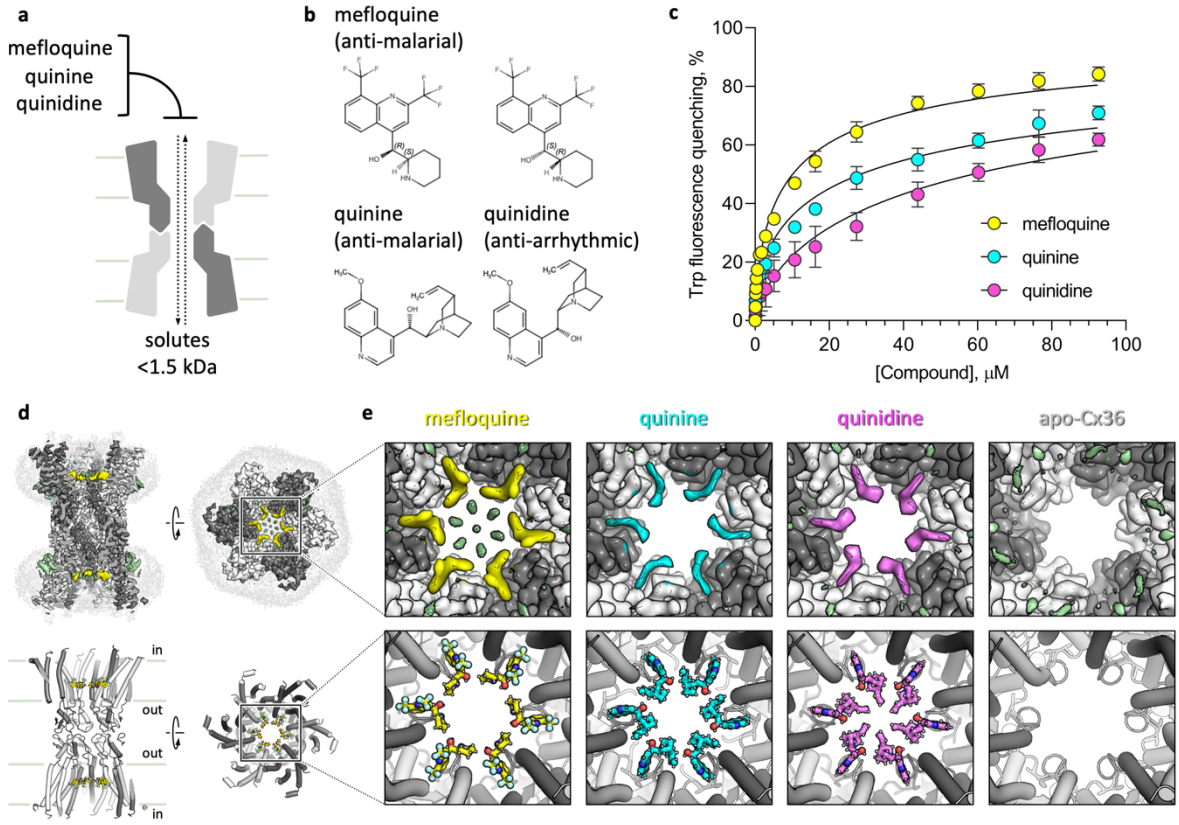

289

290

291 **Figure 1. Binding of anti-malarial drugs to Cx36. a,** A sketch illustrating the Cx36-mediated solute
292 translocation and inhibition by selected small molecules. **b,** Chemical structures of mefloquine, quinine
293 and quinidine. **c,** Tryptophan fluorescence quenching-based binding assays of three drugs with purified
294 Cx36; the apparent K_d values are 10.4 ± 1.3 μM (mefloquine), 29 ± 5.3 (quinine), 58 ± 9 (quinidine);
295 the values are expressed as mean ± S.D. (n = 3); the K_d mean values are significantly different from
296 each other, judged by one way ANOVA. **d,** Cryo-EM map (top) and model of mefloquine-bound Cx36.
297 Yellow density (top) corresponds to bound mefloquine; individual Cx36 monomer are coloured white
298 and grey, to easily distinguish monomer boundaries. The light grey density corresponds to detergent
299 micelles surrounding the membrane regions of Cx36. **e,** Zoomed-in views of maps (top) and models
300 (bottom) of the mefloquine-, quinine- and quinidine-bound Cx36 (yellow, cyan, magenta, respectively),
301 compared to the drug-free apo-Cx36 (right-most panels). All refined maps are contoured at 5σ for
302 comparison.

303

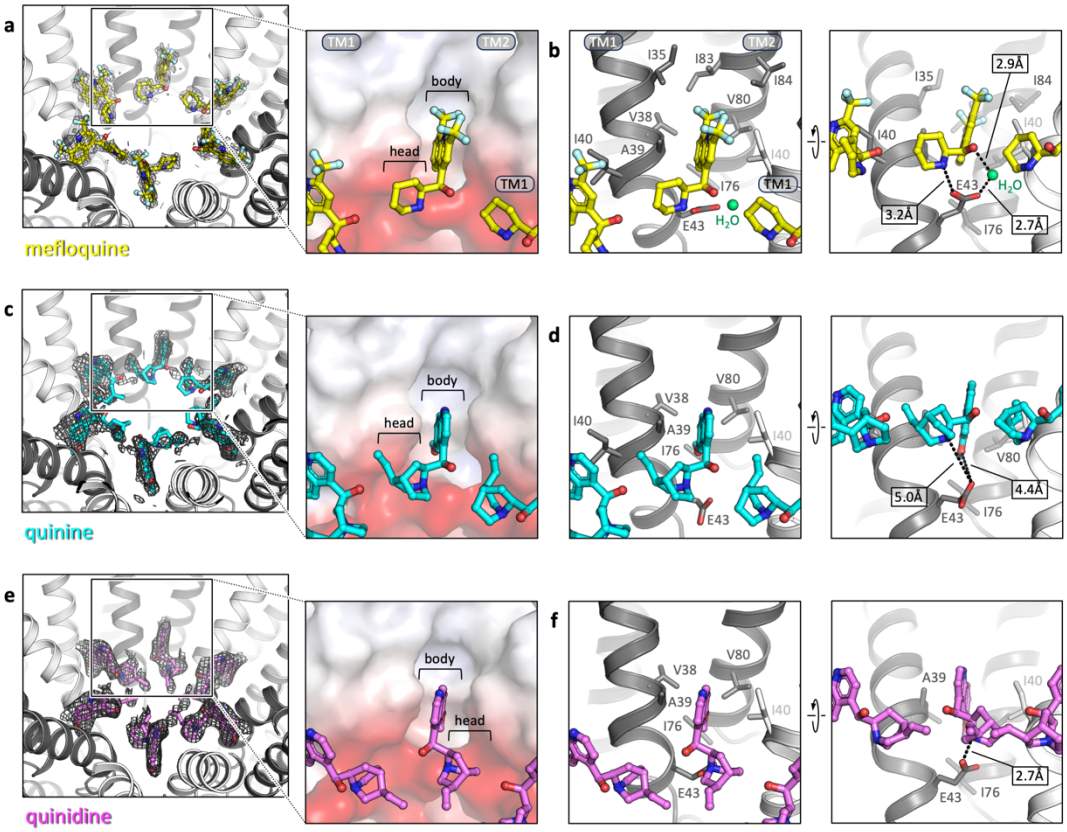

Figure 2. Molecular features of the inhibitor site in Cx36. a, Densities of six mefloquine molecules are shown as mesh (postprocessed density map, contoured at 3σ). *Inset*: the planar "body" of mefloquine is inserted into a hydrophobic groove formed by TM1 and TM2 of one Cx36 monomer and a portion of TM1 of the neighbouring Cx36 monomer; the head-group ("head") orients towards the pore, making contacts with the polar region of the TM1 and with the neighbouring mefloquine molecule. **b,** A detailed representation of the binding site residues; a water molecule linking E43 carboxyl with the hydroxy-group of mefloquine is coloured light green. *Right*: distances (Å) between the polar atoms of mefloquine and the E43 / water are shown in white boxes. **c-d, e-f,** Same as a-b, for quinine (c-d) and quinidine (e-f).

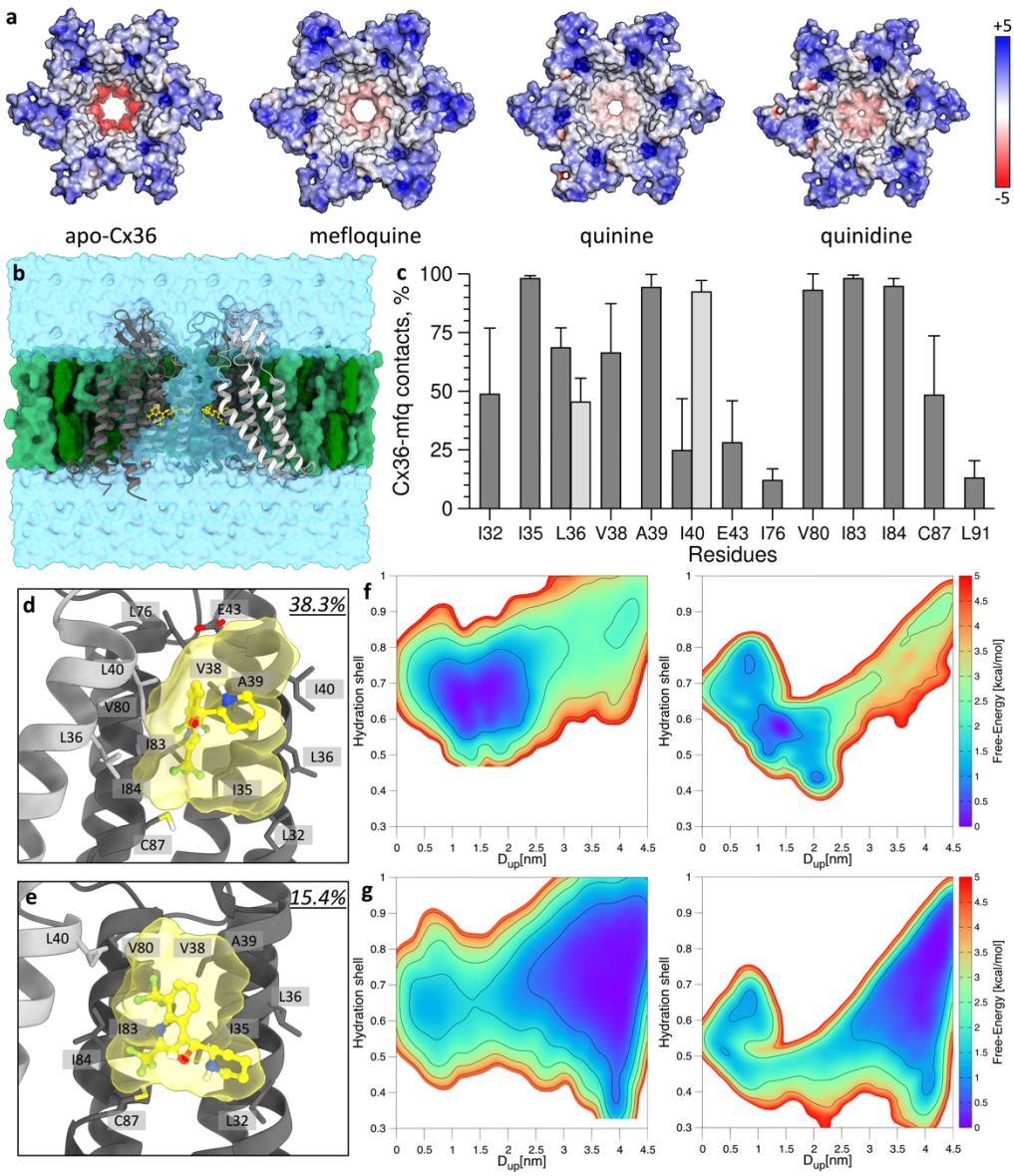

316

317 **Figure 3. Pore electrostatics and molecular dynamics of drug-bound Cx36. a,** The drug-free (apo-
318 Cx36) and drug-bound structures of Cx36, in surface representation, coloured according to electrostatic
319 potential; the scale bar corresponds to -5 / +5 kT/e. Binding of the hydrophobic drugs changes pore
320 electrostatics (mefloquine) and/or introduces a steric barrier (quinine, quinidine). **b,** Cross-section of
321 the membrane-embedded *6mfq-Cx36* hemichannel. To easily distinguish monomer boundaries,
322 individual Cx36 monomer are coloured in light and dark grey. The mefloquine molecules are coloured
323 yellow, POPC molecules - light green, and cholesterol molecules - dark green. The water content is
324 coloured transparent cyan. **c**, Average frequencies of occurrence of the contacts between Cx36
325 monomers and mefloquine molecules in the *6mfq-Cx36* MD simulations. Residues belonging to
326 different monomers are coloured in light and dark grey. The standard deviation of each point is
327 represented through the error bar. **d-e**, Interactions established by mefloquine in cluster families *C1* (**d**)
328 and *C2* (**e**). Their own frequency of occurrence during the *6mfq-Cx36* MD simulation is reported in the
329 top right corners. The solvent accessible surface of mefloquine coloured transparent yellow, whereas

330 the adjacent monomers of Cx36 are coloured dark and light grey, respectively. **f-g,** Free-energy surfaces
331 associated with K^+ (**f**) and Cl^- (**g**) permeation across the Cx36 hexamer in the *apo-Cx36* and *6mfq-Cx36*
332 systems (left and right panels, respectively). The maps are coloured according to bars on the right side,
333 while the isolines are placed every 1 kcal/mol.

334

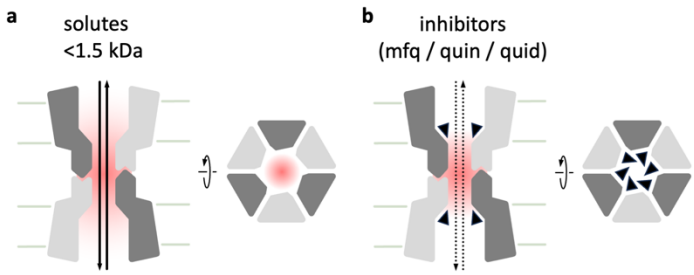

Figure 4. A structure-based model of drug-mediated Cx36 inhibition. a, Under basal conditions, Cx36 (as other connexin GJCs) is permeable to solutes with a molecular weight cut-off in the ~1-1.5 kDa range. The electrostatic properties of the pore enable solute movement. **b,** Upon drug binding as observed in our cryo-EM 3D reconstructions (mefloquine - "mfq", quinine - "quin", quinidine - "quid", shown as black triangles), steric obstruction is introduced into the path of the solutes and the electrostatic properties of the pore are altered, resulting in reduced solute flux (dotted arrows).

Supplementary Materials

Materials and Methods

Extended Data Figs. 1 to 11

Extended Data Tables 1 to 2

References (1-28)

References

1 Goodenough, D. A. & Paul, D. L. Gap junctions. *Cold Spring Harb Perspect Biol* **1**, a002576 (2009). https://doi.org:10.1101/cshperspect.a002576

2 Aasen, T. Connexins: junctional and non-junctional modulators of proliferation. *Cell Tissue Res* **360**, 685-699 (2015). https://doi.org:10.1007/s00441-014-2078-3

3 Vinken, M. Introduction: connexins, pannexins and their channels as gatekeepers of organ physiology. *Cell Mol Life Sci* **72**, 2775-2778 (2015). https://doi.org:10.1007/s00018-015-1958-3

4 Rodriguez-Sinovas, A., Sanchez, J. A., Valls-Lacalle, L., Consegal, M. & Ferreira-Gonzalez, I. Connexins in the Heart: Regulation, Function and Involvement in Cardiac Disease. *Int J Mol Sci* **22** (2021). https://doi.org:10.3390/ijms22094413

5 Zeng, W. *et al.* Downregulation of connexin 43-based gap junctions underlies propofol-induced excessive relaxation in hypertensive vascular smooth muscle cells. *Cell Commun Signal* **21**, 163 (2023). https://doi.org:10.1186/s12964-023-01176-3

6 Rohr, S. J. C. r. Role of gap junctions in the propagation of the cardiac action potential. **62**, 309-322 (2004).

7 Poelzing, S., Rosenbaum, D. S. J. A. J. o. P.-H. & Physiology, C. Altered connexin43 expression produces arrhythmia substrate in heart failure. **287**, H1762-H1770 (2004).

8 Deans, M. R., Gibson, J. R., Sellitto, C., Connors, B. W. & Paul, D. L. J. N. Synchronous activity of inhibitory networks in neocortex requires electrical synapses containing connexin36. **31**, 477-485 (2001).

9 Blatow, M. *et al.* A novel network of multipolar bursting interneurons generates theta frequency oscillations in neocortex. **38**, 805-817 (2003).

10 Pérez-Armendariz, E. M. J. N. Connexin 36, a key element in pancreatic beta cell function. **75**, 557-566 (2013).

11 Warner, A. in *Seminars in cell biology.* 81-91 (Elsevier).

12 Chan, D. K., Schrijver, I. & Chang, K. W. J. G. i. M. Connexin-26–associated deafness: Phenotypic variability and progression of hearing loss. **12**, 174-181 (2010).

13 Berthoud, V. M. *et al.* Connexin mutants compromise the lens circulation and cause cataracts through biomineralization. **21**, 5822 (2020).

14 Bortolozzi, M. J. F. i. m. n. What's the function of connexin 32 in the peripheral nervous system? **11**, 227 (2018).

15 Lillo, M. A. *et al.* Remodeled connexin 43 hemichannels alter cardiac excitability and promote arrhythmias. **155** (2023).

16 Delmar, M. & Makita, N. J. C. o. i. c. Cardiac connexins, mutations and arrhythmias. **27**, 236-241 (2012).

17 Zhou, M. *et al.* The roles of connexins and gap junctions in the progression of cancer. **21**, 1-19 (2023).

18 Bosen, F. *et al.* Altered epidermal lipid processing and calcium distribution in the KID syndrome mouse model Cx26S17F. **589**, 1904-1910 (2015).

19 Bicego, M. *et al.* Selective defects in channel permeability associated with Cx32 mutations causing X-linked Charcot–Marie–Tooth disease. **21**, 607-617 (2006).

20 Thibodeau, I. L. *et al.* Paradigm of genetic mosaicism and lone atrial fibrillation: physiological characterization of a connexin 43–deletion mutant identified from atrial tissue. **122**, 236-244 (2010).

21 Roh, D.-H. *et al.* Intrathecal injection of carbenoxolone, a gap junction decoupler, attenuates the induction of below-level neuropathic pain after spinal cord injury in rats. **224**, 123-132 (2010).

22 Zhou, J. Z. *et al.* Osteocytic connexin hemichannels suppress breast cancer growth and bone metastasis. **35**, 5597-5607 (2016).

23 Ripps, H., Qian, H., Zakevicius, J. J. C. & neurobiology, m. Properties of connexin26 hemichannels expressed in Xenopus oocytes. **24**, 647-665 (2004).

24 Guan, X. *et al.* The sleep-inducing lipid oleamide deconvolutes gap junction communication and calcium wave transmission in glial cells. **139**, 1785-1792 (1997).
25 Venance, L., Piomelli, D., Glowinski, J. & Glaume, C. J. N. Inhibition by anandamide of gap junctions and intercellular calcium signalling in striatal astrocytes. **376**, 590-594 (1995).
26 Bai, D., Del Corsso, C., Srinivas, M., Spray, D. C. J. J. o. P. & Therapeutics, E. Block of specific gap junction channel subtypes by 2-aminoethoxydiphenyl borate (2-APB). **319**, 1452-1458 (2006).
27 Söhl, G., Maxeiner, S. & Willecke, K. J. N. r. n. Expression and functions of neuronal gap junctions. **6**, 191-200 (2005).
28 Belousov, A. B. *et al.* Neuronal gap junctions play a role in the secondary neuronal death following controlled cortical impact. **524**, 16-19 (2012).
29 Belousov, A. B., Nishimune, H., Denisova, J. V. & Fontes, J. D. J. N. l. A potential role for neuronal connexin 36 in the pathogenesis of amyotrophic lateral sclerosis. **666**, 1-4 (2018).
30 Lee, S. N. *et al.* Cryo-EM structures of human Cx36/GJD2 neuronal gap junction channel. *Nat Commun* **14**, 1347 (2023). https://doi.org:10.1038/s41467-023-37040-8
31 Cruikshank, S. J. *et al.* Potent block of Cx36 and Cx50 gap junction channels by mefloquine. **101**, 12364-12369 (2004).
32 Srinivas, M., Hopperstad, M. G. & Spray, D. C. J. P. o. t. N. A. o. S. Quinine blocks specific gap junction channel subtypes. **98**, 10942-10947 (2001).
33 Margineanu, D. G. & Klitgaard, H. J. B. r. b. The connexin 36 blockers quinine, quinidine and mefloquine inhibit cortical spreading depression in a rat neocortical slice model in vitro. **71**, 23-28 (2006).
34 Wong, W. *et al.* Mefloquine targets the Plasmodium falciparum 80S ribosome to inhibit protein synthesis. **2**, 1-9 (2017).
35 Dziekan, J. M. *et al.* Identifying purine nucleoside phosphorylase as the target of quinine using cellular thermal shift assay. **11**, eaau3174 (2019).
36 Nevin, R. L., Byrd, A. M. J. N. & Therapy. Neuropsychiatric adverse reactions to mefloquine: a systematic comparison of prescribing and patient safety guidance in the US, UK, Ireland, Australia, New Zealand, and Canada. **5**, 69-83 (2016).
37 Nevin, R. L. J. P. r. & perspectives. A serious nightmare: psychiatric and neurologic adverse reactions to mefloquine are serious adverse reactions. **5**, e00328 (2017).
38 Coker, S. J., Batey, A. J., Lightbown, I. D., Díaz, M. E. & Eisner, D. A. J. B. j. o. p. Effects of mefloquine on cardiac contractility and electrical activity in vivo, in isolated cardiac preparations, and in single ventricular myocytes. **129**, 323-330 (2000).
39 Bykowski, A., Hashmi, M. F. & Logan, T. D. in *StatPearls [Internet]* (StatPearls Publishing, 2023).
40 Giustetto, C. *et al.* The Brugada syndrome: pharmacological therapy. *Eur Heart J Suppl* **25**, C32-C37 (2023). https://doi.org:10.1093/eurheartjsupp/suad036
41 Invernizzi, M. & Parrinello, M. Rethinking Metadynamics: From Bias Potentials to Probability Distributions. *J Phys Chem Lett* **11**, 2731-2736 (2020). https://doi.org:10.1021/acs.jpclett.0c00497
42 Dawson, G. R. *et al.* An inverse agonist selective for α5 subunit-containing GABAA receptors enhances cognition. **316**, 1335-1345 (2006).
43 Pexton, T., Moeller-Bertram, T., Schilling, J. M. & Wallace, M. S. J. E. o. o. i. d. Targeting voltage-gated calcium channels for the treatment of neuropathic pain: a review of drug development. **20**, 1277-1284 (2011).
44 Tabuteau, H., Jones, A., Anderson, A., Jacobson, M. & Iosifescu, D. V. J. A. J. o. P. Effect of AXS-05 (dextromethorphan-bupropion) in major depressive disorder: A randomized double-blind controlled trial. **179**, 490-499 (2022).
45 Sanguinetti, M. C. & Tristani-Firouzi, M. J. N. hERG potassium channels and cardiac arrhythmia. **440**, 463-469 (2006).
46 Laird, D. W. & Lampe, P. D. J. N. r. D. d. Therapeutic strategies targeting connexins. **17**, 905-921 (2018).